Electrofission of ^{239}Pu in the energy range 7–12 MeV

J. D. T. Arruda-Neto, M.-L. Yoneama, J. F. Dias,* F. Garcia,† M. A. V. Reigota, and V. P. Likhachev‡
Instituto de Física, Universidade de São Paulo, Caixa Postal 66318, CEP, 05315-970 São Paulo, Brazil

F. Guzmán, O. Rodriguez, and J. Mesa
Instituto Superior de Ciência y Tecnologia Nucleares, Apartado Postal 6163, Havana, Cuba
(Received 18 June 1996)

The electrofission cross section of ^{239}Pu(e,f) is measured between 7 and 12 MeV. The data are analyzed by means of the virtual photon formalism, assuming that $E1$, $E2$ $(T=0)$, and $M1$ transitions are involved. Using known estimates for the $E1$ and $E2$ $(T=0)$ fission strengths, it is deduced an $M1$ fission strength of 19 $\pm 4\mu_N^2$ concentrated near the fission barrier (between 5.4 and 5.8 MeV). The levels of the ^{239}Pu transition nucleus are theoretically obtained; a bunch of positive-parity levels shows up between 5.5 and 5.9 MeV, which might well be associated with the deduced $M1$ strength, since the $E2$ strength is negligible in this energy interval. [S0556-2813(97)04005-3]

PACS number(s): 25.30.Rw, 25.85.Jg, 24.30.Cz, 21.10.Ma

I. INTRODUCTION

The electrofission of actinide nuclei has been intensively studied in the past two decades since the seminal works of Kneissl at Giessen [1,2] and Shotter at Glasgow [3] where, for the first time, attempts were made to deduce the $E1$ and $E2$ strengths. On the other hand, the investigation of the nuclear fission process, induced by real (photofission) and virtual (electrofission) electromagnetic radiation, has benefited from the advent of the high-duty factor, continuous wave, electron accelerators. In particular, exclusive $(e,e'f)$ experiments carried out at the Mainz Microtron facility with actinide nuclei have proved to be very convenient to disentangle the fission multipolar components (mostly $E1$, $E3$, $E2$ and/or $E0$) associated with the primary excitation process [4].

However, the investigation of near- and sub-barrier fission by means of $(e,e'f)$ or tagged photon (γ,f) experiments is very difficult, particularly at energies $\omega \lesssim 6$ MeV. In fact, the very low cross sections, verified in this energy region, avoid the obtention of reasonable count rate statistics. Thus, most of the low energy data so far obtained come from inclusive bremsstrahlung- and electron-induced fission measurements. In particular, the potentialities of inclusive (e,f) experiments, for the study of multihumped fission barriers, have been recently demonstrated [5].

For odd-N and/or odd-Z nuclei there is, however, an additional difficulty: photo- and electrofission angular distributions are expected to be isotropic or near isotropic at energies somewhat above the barrier [6]. Thus, a separation of all the multipolar components (mostly $M1$, $E1$, $E2$, and/or $E0$) cannot be achieved unambiguously at low energies near the fission barrier. We note, in this regard, that for ^{235}U Weber and collaborators [4] succeeded in the separation of $E1$ from $E2$ and/or $E0$ by means of an original analysis of $(e,e'f)$ data. However, it was not possible either to disentangle $E2$ from $E0$, or to sample any $M1$ strength (details in Ref. [4]).

On the other hand, an inclusive (e,f) measurement is dominated by events near the *photon point*, because forward momentum transfers prevail—thus longitudinal components like $E0$ are *naturally* suppressed. This peculiarity is explored in this work. Actually, the complementary character of the (e,f) to the kinematically complete $(e,e'f)$ data was pointed out by one of us elsewhere [7]. More recently, however, Weber *et al.* [4,8] estimated the fission barriers of ^{238}U associated with six fission channels: $(J^\pi,K)=(0^+,0)$, $(1^-,0)$, $(1^-,1)$, $(2^+,0)$, $(2^+,1)$, and $(2^+,2)$, from exclusive $(e,e'f)$ angular correlation measurements. There is good agreement with the results for $(J^\pi,K)=(1^-,0)$, $(1^-,1)$, $(2^+,0)$, and $(2^+,1)$, obtained from the analysis of inclusive (e,f) angular distribution data previously taken at this laboratory [9].

Among odd actinides, ^{239}Pu has the smallest spin $(J_0^\pi = 1/2^+)$; thus, its transition nucleus is expected to exhibit not too many levels near the barrier, enhancing, thus, the selectivity of the multipolar components. As discussed below, this fact would provide a better evaluation of λL strengths concentrated near the fission barrier, as, e.g., $M1$.

A quite complete and recent review on low-energy electro- and photofission of actinides could be found in Ref. [10], to which the reader is referred.

A. Low energy photofission

For photon energies $\omega \lesssim 40$ MeV, photoabsorption takes place by means of the excitation of nuclear collective modes (the well known giant multipole resonances). In addition, pre-equilibrium emission is negligible (as discussed in [11]) and, as a consequence, the photofission cross section is

$$\sigma_{\gamma,f}(E_x)=\sigma_{\mathrm{CN}}(E_x)P_f(E_x), \tag{1}$$

where σ_{CN} is the cross section for compound nucleus forma-

*Permanent address: Instituto de Física-UFRGS, Porto Alegre (RS), Brazil.

†Permanent address: ISCTN, apartado postal 6163, Havana, Cuba.

‡On leave from Kharkov Institute of Physics and Technology, Ukraine.

tion with excitation energy E_x, and P_f is its fission probability. Moreover, in this energy region the following approximations are valid [11]:

$$\sigma_{\mathrm{CN}} = \sigma_T \quad \text{and} \quad E_x = \omega, \tag{2}$$

where σ_T is the total photoabsorption cross section. Therefore, the photofissility $\sigma_{\gamma,f}/\sigma_T$ is equal to the compound nucleus fission probability P_f.

The photofissility of actinide nuclei for $\omega \lesssim 20$ MeV, which is mostly associated with the fission decay of the giant dipole resonance (GDR), has been systematically measured with monochromatic photons. A few MeV above the fission barrier ($\omega \gtrsim 8$ MeV) P_f, in general, is a somewhat flat function of ω up to the second-chance fission threshold (B_{nf}), while for $\omega > B_{nf}$ P_f is a moderately increasing function of ω. Thus, the shape of the experimentally obtained (γ,f) cross section is nearly proportional to σ_T [12]. Given the fact that the properties of the GDR are well known, further photofission studies in this energy region are not stimulating.

At energies near the fission barrier ($\omega \lesssim 8$ MeV), the fission probability reveals aspects associated with the barrier parameters (its height, in particular) and with the nuclear level densities as well [13]. Also, at $\omega \lesssim 8$ MeV, one might expect to find only the low energy tail of the giant resonances, particularly the GDR and the isoscalar giant quadrupole resonance (GQR). In this case, therefore, the photofission cross section behavior with ω reflects that of P_f.

B. Level distribution at the saddle point

The level sequence at the saddle point of even-even actinides is the same as that built over the ground state, but the level spacing is slightly different and it is a function of the nuclear deformation (see, e.g., Refs. [6] and [14]). Thus, for electromagnetic excitations near the fission barrier, where $E1$ and $E2$ transitions are dominant, fission takes place only through a few (J^π,K) channels: $(1^-,0)$, $(1^-,1)$, and $(2^+,0)$, mostly. In ^{238}U, for example, only a single $(1^+,1)$ level shows up near the barrier [6]; this level with positive parity could be populated only by means of $M1$ excitations.

However, the situation is different for odd-mass-number nuclei, since their levels at the saddle point (identified as the Nilsson states of a deformed potential) are much more ''densely'' distributed; also, the level sequence is different from that near the ground state [6,14].

^{239}Pu is a particularly interesting nucleus to study since, up to ≈ 0.4 MeV above the ground state, all levels have positive parity $(1/2^+,3/2^+,5/2^+,\ldots)$ while from ≈ 0.4 MeV to ≈ 0.5 MeV the majority of levels has negative parity [15]. There has been no experimental or theoretical evidence of the existence of positive- and/or negative-parity bunches of levels near the saddle point. Positive-parity levels of the transition nucleus are populated by $E2$ and/or $M1$ photoexcitation. Thus the experimental observation of $E2$ and/or $M1$ concentration of strength, in the vicinity of the saddle point, would be compelling evidence supporting the existence of positive-parity bunches of levels. In addition, it would be quite useful to perform complete calculations for the low-lying levels of the transition nucleus (see Sec. III D).

C. Low energy $E2$ $(T=0)$ fission strength

From the theoretical point of view we note that detailed statistical model calculations have been successful in describing the fission decay of even-even actinides following excitation of $E\lambda$ giant multipole resonances [13]. Realistic level densities and the levels of the transition state nucleus were used in an exemplifying calculation for ^{236}U and it was found that the GQR fission decay probability is as large as that of the GDR at energies $\omega \gtrsim 8$ MeV. At energies close to the fission barrier, the GQR fission probability was found to be appreciably larger than that of the GDR, while the $E0$ giant resonance fission probability followed closely that of the GQR (details in Ref. [13]). This is an indication that (a) the densities of levels, populated by $E1$ and $E2$ transitions at the saddle point, are different; and that (b) the same would occur with the levels of the residual nucleus (formed after one neutron emission) altering, thus, the $(\gamma,f)/(\gamma,n)$ competition.

In fact, photo- and electrofission-fragment angular distribution data, systematically taken for even-even actinides, have demonstrated the existence of substantial $E2$ fission strength at energies just above the fission barrier. A detailed discussion on this issue is found in Refs. [9,16]. Regarding odd actinides, low energy data are less abundant and more difficult to analyze, due to the lack of fission angular distributions. Moreover, even for ^{239}Pu, where low-energy (γ,f) angular distributions have been measured for three decades [17,18], it was not possible to obtain information on multipolar transitions because, for odd nuclei, the anisotropies are sensitive only to K (the angular momentum projection on the nuclear symmetry axis), regardless of any particular J^π [6]; this issue is retaken in Sec. III E. However, electrofission studies carried out for ^{233}U, ^{235}U, and ^{237}Np have indicated the presence of substantial fractions of GQR strength near the fission barrier [19–21].

D. $M1$ strength near the fission barrier

In the past decade, the study of magnetic dipole excitations of nuclei attracted much interest in low energy nuclear physics. Indeed, with the work of Bohle and collaborators [22], (e,e') and later (γ,γ') and (p,p') experiments [23] proved to be powerful tools for the investigation of the nuclear orbital and spin magnetic dipole response in nuclei. In particular, a clear picture concerning the features of the magnetic dipole response in rare earth nuclei could be drawn. However, the study of the $M1$ giant resonance in actinide nuclei has been restricted to few cases [24].

Indeed, the issue of the existence of a giant magnetic dipole resonance (GMDR) has been the subject of much experimental and theoretical work (an excellent and comprehensive review on this issue is presented in Ref. [25]). In fact, it seems that only for $M1$ transitions in $A \lesssim 60$ nuclei one can see any semblance of a GMDR. Thus, with the probable exception of $M1$ transitions in heavy nuclei, magnetic transitions do not manifest obvious resonances of the type exhibited by giant electric modes. We note, in this regard, that (n,γ) [26] and resonance fluorescence [27] measurements appear to have succeeded in identifying compact giant $M1$ resonances in ^{208}Pb and in other heavy closed-shell nuclei.

TABLE I. $M1$ strength for heavy nuclei.

Nucleus	Strength (units of μ_N^2)	Peak (MeV)	Reference
^{234}U	5.8 ± 1.8	6.4 ± 0.3	[51]
^{236}U	4.0 ± 1.2	5.8 ± 0.2	[51]
^{238}U	4.1 ± 1.8	6.5 ± 0.3	[51]
^{233}U	18 ± 5	6.3 ± 0.3	[19]
^{235}U	16 ± 4	6.0 ± 0.4	[20]
^{237}Np	18 ± 4	6.2 ± 0.3	[21]
^{239}U	18.5	6.5	[52]
^{208}Pb	15.6	Fragmented	[27]

From the experimental point of view, however, it is very difficult to obtain reliable information on $M1$ transitions in heavy nuclei from, e.g., single-arm (e,e') experiments, even at backward scattering angles [28]. The main difficulty comes from the fact that an (e,e') measurement samples the strength function at $q>\omega$, and the extrapolation of the form factor back to the photon point $(q=\omega)$ is a tedious and uncertain enterprise.

On the other hand, an inclusive (e,f) reaction is dominated by small-momentum-transfer events; thus electrofission measurements correspond to measurements near the photon point. We have been exploring this peculiarity in a systematic investigation of $M1$ strength concentrations near the fission barrier of several actinide nuclei (see Table I). These have been the only experimental information so far obtained for $M1$ transitions in the actinide region.

From the results shown in Table I we note that the energy centroids ω_c of the $M1$ transition strengths lie within the range $35-40\,A^{-1/3}$ MeV [25,26], which for ^{239}Pu corresponds to 5.6–6.5 MeV with a width $\approx$1–1.5 MeV] $(\approx 0.2\omega_c)$. Also quite interesting is the fact that the $M1$ strengths observed in odd actinides are about four times more intense than those observed in even actinides (see Table I); this could be due to the existence of several positive-parity levels bunched near the fission barrier of odd actinides, while for even actinides only one $(1^+,1)$ level at equilibrium has been reported (Ref. [6], p. 42). Such a possibility is checked in the present work for ^{239}Pu, both experimentally and theoretically.

E. Aim of the present work

The general aim of the present work is to measure, for the first time, the electrofission cross section of ^{239}Pu at low and near-barrier energies.

More specifically, a data analysis will be carried out in order to deduce a possible concentration of $M1$ strength near the fission barrier of ^{239}Pu. To this end, it is used as input of the calculations: (a) the well-known $E1$ photofission cross section of ^{239}Pu [12]; (b) the parameters of the GQR $(T=0)$ taken from the literature [29]—actually, only an estimate of the GQR $(T=0)$ low energy tail is necessary; and (c) fission probabilities obtained from the statistical model for the fission process.

In order to check the consistency of the results, we work out a detailed calculation of the ^{239}Pu transition nucleus levels (J^π,K). The reliability of these calculations will also be checked through their comparison with photofission angular distributions of ^{239}Pu found in the literature.

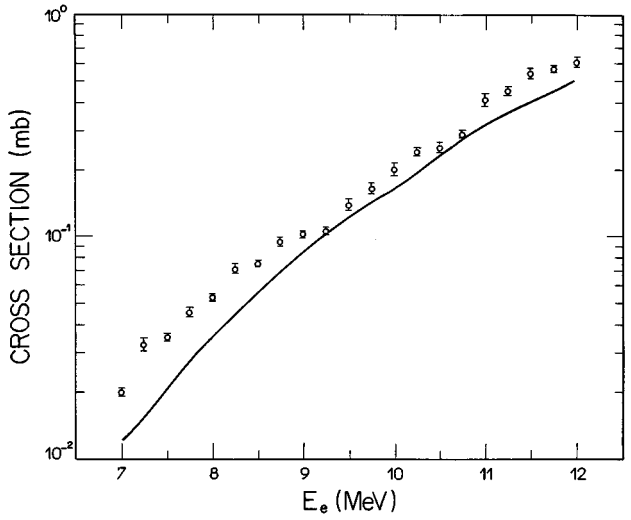

FIG. 1. Data points: electrofission cross section $\sigma_{e,f}$ for ^{239}Pu as a function of the incident electron energy. The uncertainties for the data points are of the order of 5%. The solid curve was obtained by integrating the measured photofission cross section from Ref. [12] with the $E1$ virtual-photon spectrum of Zamani-Noor and Onley [31].

II. EXPERIMENT AND RESULTS

The absolute electrofission cross section $\sigma_{e,f}$ of ^{239}Pu was measured, for the first time, at the University of São Paulo Electron Linear Accelerator for electron energies E_e ranging from 7 to 12 MeV, in small steps of 0.25 MeV. Mica foils were used as fission detectors (100% efficiency). For irradiations in the interval 7–9 MeV, 12 mica foils $(2\times2\ \mathrm{cm}^2)$ were positioned around the target, 20 cm from its center, covering the angular range 10°–100° with respect to the incident beam direction. No statistically significant anisotropy was observed. The beam was monitored, before hitting the target, by a ferrite core toroid and, simultaneously, by a Faraday cup after hitting the target. The thickness of the ^{239}Pu target $(\approx 650\ \mu g/\mathrm{cm}^2)$ was measured by a conventional alpha-counting method. There was negligible γ ray contamination of the electron beam. Other background sources, resulting from room-returned thermal neutrons and gammas and scattered electrons, were experimentally shown to be negligible. In particular, the significance of fission induced by neutron background was checked using the same procedure described in the appendix of Ref. [30]; it corresponds for ^{239}Pu to less than 0.5% of the total electrofission yield. Details of the accelerator, reaction chamber, monitoring devices, detection techniques and procedures can be found in Refs. [9] and [30].

Figure 1 shows our results for the electrofission cross section of ^{239}Pu, which can be expressed by

$$\sigma_{e,f}(E_e)=\sum_{\lambda L}\int_0^{E_e}\sigma_{\gamma,f}^{\lambda L}(\omega)N^{\lambda L}(E_e,\omega)\,\frac{d\omega}{\omega}, \qquad (3)$$

where $N^{\lambda L}(E_e,\omega)$ is the virtual photon spectrum calculated in the DWBA with nuclear size effect corrections [31], λL

indicates the multipolar character of the transition, and $\sigma_{\gamma,f}^{\lambda L}(\omega)$ is the partial λL-photofission cross section; thus the total photofission cross section is

$$\sigma_{\gamma,f}(\omega)=\sum_{\lambda L}\sigma_{\gamma,f}^{\lambda L}(\omega). \tag{4}$$

We would like to stress that the disentangling of the λL strengths cannot be performed unambiguously in an inclusive (e,f) experiment. However, if among two or three λL components just one of them is unknown, as in near-barrier data, it is possible to take advantage of different energy distributions and thresholds of the λL strengths in order to obtain a reasonable separation, as shown below.

The kinematics of this experiment allow us to assume that the main components in the 7–12 MeV range certainly are $E1$, $E2$ $(T=0)$, and $M1$ (see discussion above); thus, from Eq. (3) we have that

$$\sigma_{e,f}(E_e)=\int_0^{E_e}[\sigma_{\gamma,f}^{E1}(\omega)N^{E1}(E_e,\omega)+\sigma_{\gamma,f}^{E2}(\omega)N^{E2}(E_e,\omega)+\sigma_{\gamma,f}^{M1}(\omega)N^{M1}(E_e,\omega)]\,\frac{d\omega}{\omega}, \tag{5}$$

and, from Eq. (4),

$$\sigma_{\gamma,f}(\omega)=\sigma_{\gamma,f}^{E1}(\omega)+\sigma_{\gamma,f}^{E2}(\omega)+\sigma_{\gamma,f}^{M1}(\omega). \tag{6}$$

Combining Eqs. (5) and (6) we obtain

$$\begin{aligned}\Delta\sigma_{e,f}(E_e)&\equiv\sigma_{e,f}(E_e)-\int_0^{E_e}\sigma_{\gamma,f}(\omega)N^{E1}(E_e,\omega)\,\frac{d\omega}{\omega}\\&=\int_0^{E_e}\sigma_{\gamma,f}^{E2}(\omega)[N^{E2}(E_e,\omega)-N^{E1}(E_e,\omega)]\,\frac{d\omega}{\omega}\\&\quad+\int_0^{E_e}\sigma_{\gamma,f}^{M1}(\omega)[N^{M1}(E_e,\omega)-N^{E1}(E_e,\omega)]\,\frac{d\omega}{\omega}.\end{aligned} \tag{7}$$

The full curve in Fig. 1 represents the term $\int_0^{E_e}\sigma_{\gamma,f}(\omega)N^{E1}(E_e,\omega)(d\omega/\omega)$ appearing in Eq. (7), which was obtained by numerical integration of the $\sigma_{\gamma,f}(\omega)$ measured at Livermore by Berman and collaborators [12] with the $E1$ virtual photon spectrum.

A mere visual inspection of Fig. 1 does not allow to draw any conclusions about the statistical and physical meanings of the electrofission cross section difference $\Delta\sigma_{e,f}$ in Eq. (7). In this regard, Fig. 2 shows the ratio

$$R(E_e)=\frac{\displaystyle\int_0^{E_e}\sigma_{\gamma,f}(\omega)N^{E1}(E_e,\omega)\,\frac{d\omega}{\omega}}{\sigma_{e,f}(E_e)}. \tag{8}$$

We note that $R(E_e)=K$ (const) only for a pure $E1$ process since, in this case,

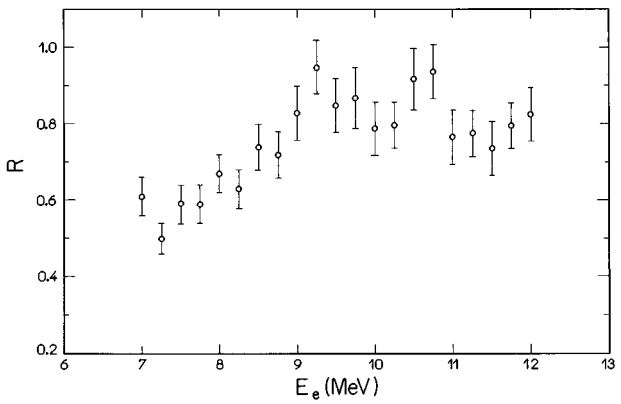

FIG. 2. Ratio of the $E1$ electrofission cross section to the total electrofission cross section for ^{239}Pu as a function of the electron energy.

$$\sigma_{e,f}(E_e)=\int_0^{E_e}\sigma_{\gamma,f}(\omega)N^{E1}(E_e,\omega)\,\frac{d\omega}{\omega}. \tag{9}$$

In addition, the magnitude of K (for pure $E1$ processes) would be the consequence of normalization differences between the São Paulo data $(\sigma_{e,f})$ and the Livermore data $(\sigma_{\gamma,f})$. However, the strong dependence of $R(E_e)$ on E_e, particularly at low energies (see Fig. 2), led us to the conclusion that sizeable multipolar components other than $E1$ must be contributing to the photofission process, in all likelihood $E2$ and $M1$.

Regarding to normalization differences between São Paulo and Livermore, they were checked for ^{239}Pu and for all the actinides so far investigated at this Laboratory, using the procedures described at length in Refs. [32] and [33]. The mean normalization factor is $\approx 2\%$, and was already taken into account for the quantities shown in Fig. 1. As discussed below, however, this is a minor source of uncertainties as regarding the main conclusions of this work.

We reproduce in Fig. 3 the restricted 7–9 MeV interval of Fig. 1, using a linear scale, where the physical meaning of $\Delta\sigma_{e,f}$ can be better appraised (see also Fig. 7). Since $\Delta\sigma_{e,f}$ is the difference between the total (e,f) cross section and the corresponding $E1$ component, this quantity is composed of the $M1$ and $E2$ $(T=0)$ components only; there is no other possible interpretation. Therefore, the least we can state up to this point is that a substantial ''non-electric-dipole'' electrofission component has been detected. Fortunately, literature indicates that a possible $M1$ resonance might well be located near the fission barrier of ^{239}Pu (see Sec. I D), that is, in the region corresponding to the low energy tail of the GQR $(T=0)$ which, as a consequence, enable us to perform the deduction of the $M1$ component with some confidence.

III. DATA ANALYSIS AND INTERPRETATION

The key quantity for our data analysis and interpretation is the electrofission cross section difference $\Delta\sigma_{e,f}$ [Eq. (7) and Figs. 3 (inset) and 7], particularly for $E_e \lesssim 8$ MeV (see below). By a simple visual inspection of the cross sections ratio $R(E_e)$ shown in Fig. 2, we get

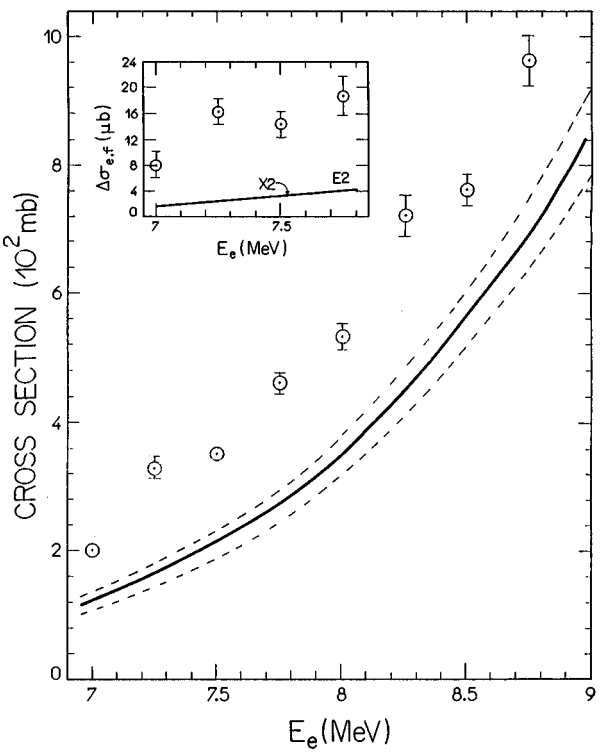

FIG. 3. Data points: linear plot of the electrofission cross section for ^{239}Pu (Fig. 1) in the energy region between 7 and 9 MeV. Solid curve: same as in Fig. 1 (the dashed lines represent the uncertainty of the calculation). Inset: electrofission cross section difference $\Delta\sigma_{e,f}$ (data points) and the $E2$ contribution (solid curve).

$$\Delta\sigma_{e,f} \approx 0.4 \text{ to } 0.5\sigma_{e,f}, \quad E_e \lesssim 8 \text{ MeV}. \tag{10}$$

Thus, even if we double the uncertainties associated with the determination of the $E1$ component (full curve in Fig. 3), we still obtain a sizeable $\Delta\sigma_{e,f}$. We cannot find, either from the $E1$ estimate or from the experiment itself, any reasonable source of uncertainties able to account for the cross section difference $\Delta\sigma_{e,f}$. Therefore, this is a significant quantity representing (e,f) components other than $E1$.

The second point we want to stress, once again, is that only $M1$ and $E2$ $(T=0)$ transitions are associated with $\Delta\sigma_{e,f}$. From them, we show below that only $M1$ is significant at lower energies, since only the low-energy tail of the GQR $(T=0)$ is contributing to the whole process. Thus, even a crude estimate of the GQR $(T=0)$ strength, and of its fission decay probability, do not alter our main conclusions about the $M1$ component, as demonstrated by the calculations shown in the following sessions.

Since, in general,

$$\sigma_{\gamma,f}^{\lambda L}(\omega) = \sigma_T^{\lambda L}(\omega) P_f^{\lambda L}(\omega), \tag{11}$$

where $\sigma_T^{\lambda L}$ is the λL-photoabsorption cross section, and $P_f^{\lambda L}$ is the corresponding fission decay probability, only a fraction of the λL strength is observed in the fission channel, particularly at energies near the fission barrier (where $P_f^{\lambda L} < 1$). Thus, it would be useful to perform estimates of the λL-fission probabilities, but this issue is not crucial for the final purposes of this work.

A. Calculation of fission probabilities

Considering high-Z nuclei and excitation energies E_x below the second-chance fission threshold (≈ 12 MeV), the fission probability is simply given by

$$P_f(E_x) = \frac{\Gamma_f(E_x)}{\Gamma_f(E_x) + \Gamma_n(E_x)}, \tag{12}$$

where Γ_f and Γ_n are the widths for fission and emission of neutrons, respectively.

With respect to the above mentioned λL-fission probability $P_f^{\lambda L}$ [Eq. (11)], it is necessary to add a few more basic comments. Possible *memory effects* related to the entrance channel are unlikely. In fact, the amplitude of the giant resonances is not sufficiently large to strongly drive the fission process (to induce a noticeable direct fission width, for example). The energy of motion of the two oscillating nuclear fluids (protons and neutrons) must be damped into the compound nucleus and reappear as deformation energy before fission can take place. Therefore, possible marked differences among the $P_f^{E\lambda}$'s could only be found near the barrier, as shown in the work of Dias *et al.* [13].

We performed calculations of P_f [Eq. (12)] using the statistical model approach developed by Vandenbosch and Huizenga [6], where it is assumed that the level density $\rho(E_x)$ is given by the so-called Fermi gas expression,

$$f(E_x) = \frac{\sqrt{\pi}}{12} a^{-1/4} E_x^{-5/4} \exp[2(aE_x)^{1/2}], \tag{13}$$

where a is the level density parameter. In this case, after dropping some small terms and expressing the nuclear radius by $R = 1.2A^{1/3}$ (fm) we obtain, for ^{239}Pu, the expression

$$\frac{\Gamma_n}{\Gamma_f} = \frac{10.7r(E_x - B_n)}{2(ra_n)^{1/2}(E_x - B_f)^{1/2} - 1} \times \exp[2a_n^{1/2}[(E_x - B_n)^{1/2} - r^{1/2}(E_x - B_f)^{1/2}]], \tag{14}$$

where $r = a_f/a_n$ is the ratio of the level-density parameter at the fission saddle point to that of the residual nucleus after neutron evaporation, B_n is the neutron binding energy and B_f is the fission barrier. The fission barrier deduced from a (γ,f) experiment mostly corresponds to the barrier for fission following $E1$ excitation. For ^{239}Pu, $B_f = 5.8$ MeV [6,12] which, in fact, represents the ''effective barrier.''

The level spacing parameter a_n was obtained from an expression proposed by Iljinov *et al.* [34], which incorporates corrections due to excitation energy and shell effects. For the parameter $r = a_f/a_n$, however, we know that both their values and energy dependence are not well defined in the literature; thus we decided to obtain it from a fitting procedure, as described below.

The fission probability obtained from (γ,f) measurements can be interpreted as an $E1$-related quantity (P_f^{E1}), which is shown in Fig. 4 for ^{239}Pu. We fitted the expression [see Eq. (12)]

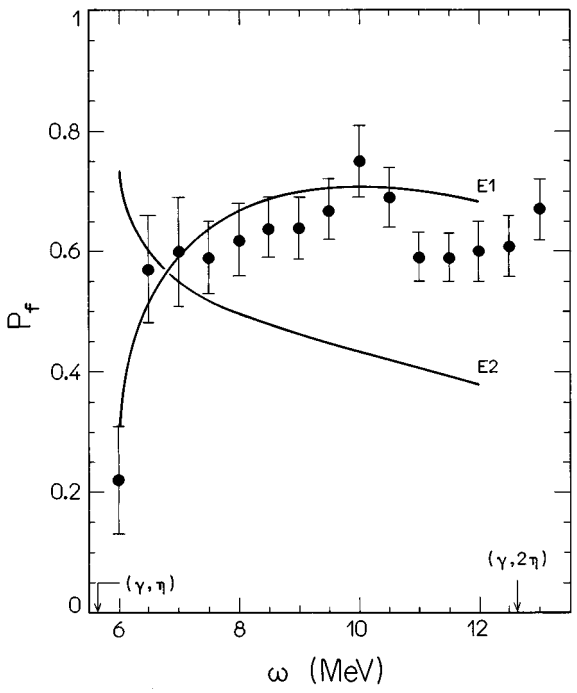

FIG. 4. Data points: experimental photofission probability obtained from Ref. [12]. The solid curves labeled $E1$ and $E2$ represent, respectively, the dipole P_f^{E1} and the quadrupole P_f^{E2} fission probabilities obtained theoretically (for more details see text).

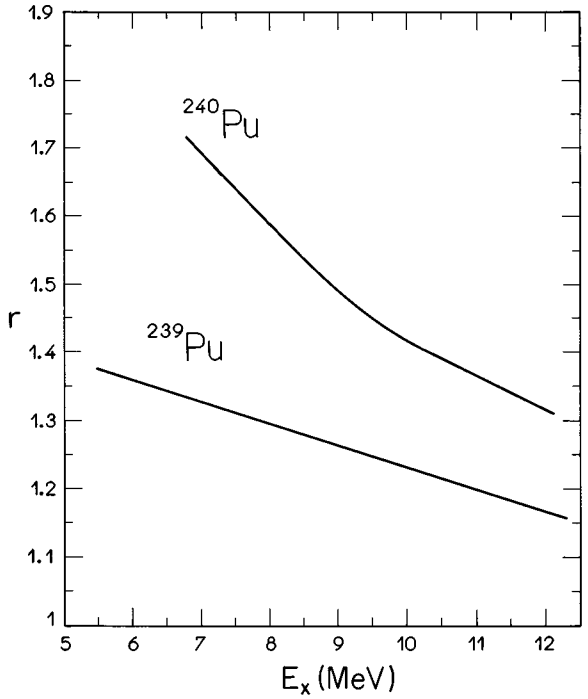

FIG. 5. Ratio of the level density parameter ($r=a_f/a_n$) for ^{239}Pu (present work), and for ^{240}Pu [6] at the fission saddle point to the level density parameter of the residual nucleus after neutron evaporation as a function of excitation energy E_x.

$$P_f^{E1}(\omega)=\frac{\Gamma_f/\Gamma_n}{1+\Gamma_f/\Gamma_n} \tag{15}$$

to the experimental data (Fig. 4), using $r=r(\omega)$ as the fitting parameter; Γ_f/Γ_n is given by Eq. (14) with $E_x=\omega$, $B_n=5.65$ MeV [12], and $B_f=5.8$ MeV. The best fit was achieved for $r(\omega)=1.48-0.0238\omega$, which is a moderate decreasing function of the energy. This result for ^{239}Pu is shown in Fig. 5 with that for ^{240}Pu [6].

In order to estimate P_f^{E2} we assumed that $r(\omega)$ is the same as that one obtained for P_f^{E1}. Regarding the fission barrier for the $E2$ fission decay we put, tentatively, $B_f=5.5$ MeV, which corresponds to the lowest positive-parity level we calculated for ^{239}Pu (see Sec. III D). The results are also shown in Fig. 4.

We note that assuming the same $r(\omega)$, for the calculation of P_f^{E1} and P_f^{E2}, is equivalent to assume that the densities of positive- and negative-parity levels are approximately the same, which is reasonable for odd actinides. Thus the peculiarities of the energy dependence of P_f^{E1} and P_f^{E2} are dictated only by their corresponding fission barriers. The situation is different for even-even actinides, where the level densities also play a significant role (see discussion in Ref. [13]).

B. Estimate of the $E2$ ($T=0$) fission strength

The $E2$ ($T=0$) photofission cross section is given by [see Eq. (11)]

$$\sigma_{\gamma,f}^{E2}(\omega)=\sigma_T^{E2}(\omega)P_f^{E2}(\omega), \tag{16}$$

where σ_T^{E2} is the $E2$ ($T=0$) photoabsorption cross section. The $E2$ ($T=0$) fission probability P_f^{E2} is shown in Fig. 4. We know from the long-wavelength approximation that [35,36]

$$\sigma_T^{E2}(\omega)=3.09\times10^{-6}\omega^3\,\frac{dB(E2;\omega)}{d\omega}\,(\text{mb}), \tag{17}$$

where ω is in MeV. The $E2$ strength function $dB/d\omega$ (in fm^4/MeV) is well described by a Breit-Wigner curve [36] with the following parameters [20]: (a) peak at 9 MeV; (b) width of 4 MeV; and (c) area equal to 100% of one $E2$ ($T=0$) EWSR unit for ^{239}Pu. As discussed below, the deduction of the $M1$ strength near the fission barrier relies on a fair estimate of the GQR low-energy tail ($\omega\lesssim7$ MeV). In this regard, we show in Fig. 6 (inset) the result of our calculation for σ_T^{E2} [Eq. (17)] using the GQR parameters mentioned above (solid line), and a calculation for σ_T^{E2} using the $E2$ strength function $dB/d\omega$ obtained from a QRPA approach for ^{238}U [54]. The agreement between the two results in the range 5–7 MeV is reasonable.

The result of our calculation for $\sigma_{\gamma,f}^{E2}$ is shown in Fig. 6, and its integration with the kernel $[N^{E2}(E_e,\omega)-N^{E1}(E_e,\omega)]$ gave us the $E2$ labeled curve of Fig. 7 [see also Eq. (7)].

For a better appraisal of the relative importance of the $E2$ component in the low-energy (e,f) process, we refer the reader to the inset shown in Fig. 3. Quite revealing is the fact that the $E2$ component is nearly *one order of magnitude* smaller than $\Delta\sigma_{e,f}$. Even by drastically changing the

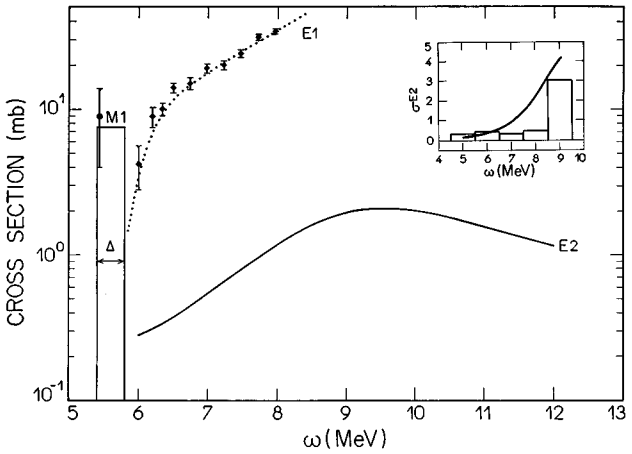

FIG. 6. Calculated $M1$ and $E2$ photofission cross sections as a function of photon energy ω (MeV). See text for details. Data points: total photofission cross section of ^{239}Pu measured by de Moraes and Cesar [53] (full circle) and Berman *et al.* [12] (full diamonds). The dotted curve labeled $E1$ is only to guide the eyes. Inset: total $E2$ photoabsorption cross sections σ_T^{E2} for ^{239}Pu (solid line; this work) and ^{238}U (histogram); the latter was obtained from QRPA calculations for the $E2$ strength [54].

GQR ($T=0$) parameters (peak and width) and the $E2$ fission probability P_f^{E2}, this one order magnitude difference does not change appreciably.

Therefore, we came easily to the conclusion that, besides $E1$ and $E2$, another multipolar component, with nearly all of its strength concentrated near the barrier, is contributing to the electrofission process. The kinematics of this experiment place the $M1$ transition as the only possible candidate.

C. The $M1$ fission strength

Equation (7) can be rewritten in the following way:

$$\Delta\sigma_{e,f}(E_e)=\Delta\sigma_{e,f}^{E2}(E_e)+\Delta\sigma_{e,f}^{M1}(E_e), \tag{18}$$

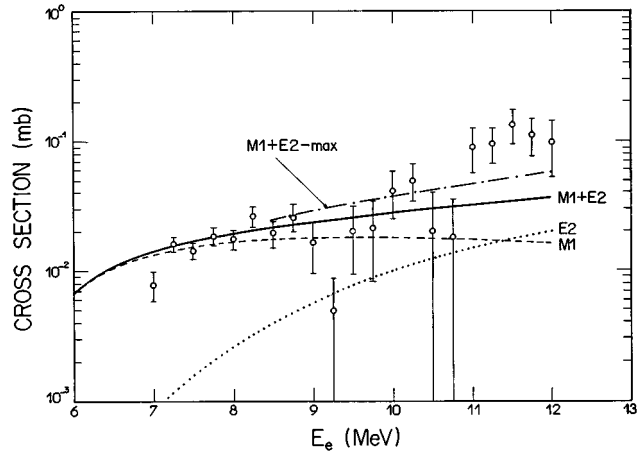

FIG. 7. Data points: electrofission cross section difference $\Delta\sigma_{e,f}(E_e)$ between $\sigma_{e,f}$ and the solid curve shown in Fig. 1. The dotted and dashed curves were calculated assuming that the transitions having multipolarity other than $E1$ are purely $E2$ and $M1$, respectively. The full curve corresponds to the calculated $E2$ strength with the addition of the $M1$ strength. The dot-dashed curve represents the calculated $E2$ strength (assuming that $P_f^{E2}=1$) plus the $M1$ strength.

where

$$\Delta\sigma_{e,f}^{M1}(E_e)=\int_0^{E_e}\sigma_{\gamma,f}^{M1}(\omega)[N^{M1}(E_e,\omega)-N^{E1}(E_e,\omega)]\,\frac{d\omega}{\omega}, \tag{19}$$

and the $E2$ contribution, $\Delta\sigma_{e,f}^{E2}$, calculated in the way described in Sec. III B, is shown in Fig. 7 (dotted curve) and in the inset of Fig. 3. The calculations show that $\Delta\sigma_{e,f}^{E2}$ is very small for $E_e\lesssim 8$ MeV; thus, in this energy range, $\Delta\sigma_{e,f}(E_e)\approx\Delta\sigma_{e,f}^{M1}(E_e)$.

A mere visual inspection of Fig. 7 shows that the $M1$ contribution to the (e,f) process, $\Delta\sigma_{e,f}^{M1}$, must be a flat function of E_e in the interval 7–12 MeV, in order to fit the experimental data. Given the integral nature of this quantity [Eq. (19)], such a flat behavior is reproduced only by means of a narrow $M1$ photofission cross section $\sigma_{\gamma,f}^{M1}$ located mostly below 6 MeV. In addition, this low-energy and narrow concentration of $M1$ strength makes $\Delta\sigma_{e,f}^{M1}$ sensitive only to the area of $\sigma_{\gamma,f}^{M1}$, for $E_e\gtrsim 7$ MeV. Thus, it is reasonable to describe $\sigma_{\gamma,f}^{M1}$ as a flat function of ω, like a histogram Δ MeV wide and with a height equal to $\sigma_{\gamma,f}^{M1}=$const. This histogram was fitted to the experimental data through the integral cross section $\Delta\sigma_{e,f}^{M1}$ [Eq. (19)], producing the curve labeled $M1$ in Fig. 7. The best fit was achieved for $\sigma_{\gamma,f}^{M1}=7.5\pm 1.1$ mb and $\Delta=0.40\pm 0.05$ MeV in the interval 5.4–5.8 MeV.

In our approximation, the $M1$-fission strength, represented by $[B\uparrow(M1)]P_f^{M1}$, is proportional to the $M1$ cross section area $\Delta\times\sigma_{\gamma,f}^{M1}$. By assuming that $P_f^{M1}\approx P_f^{E2}$ (since the barriers are similar) we deduced

$$\left[\frac{B\uparrow(M1)}{\mu_N^2}\right]=19\pm 4, \tag{20}$$

where μ_N is the nuclear magneton, and $B\uparrow(M1)$ is the integrated $M1$ strength function $dB\uparrow/d\omega$ [37]. In the hypothetical possibility where $P_f^{M1}<P_f^{E2}$, the $M1$ strength given by Eq. (20) would represent a lower limit.

Also, we would like to add a final comment on the issue related both to the $E2$ strength, calculated in this work for $\omega\lesssim 7$ MeV, and the determination of the $M1$ strength. We note, in this sense, that the calculated $E2$ strength does not play a significant role. In fact, by repeating our calculations with an $E2$ strength *three times larger* than that obtained in the first place (see the inset of Fig. 6), we deduced an $M1$ strength $\approx 22\%$ smaller, that is, $B\uparrow(M1)\approx 15\mu_N^2$, which would not change appreciably our main conclusions (see below).

It is important to stress that we are by no means saying that this is the only $M1$ strength contributing to the (e,f) process up to 12 MeV. We are just saying that this is the $M1$ strength concentrated near the fission barrier of ^{239}Pu, which might well be associated with a bunch of positive-parity levels in the saddle point of ^{239}Pu [as discussed below in Sec. III D]. Because of the fast onset of $E1$ and $E2$ ($T=0$) for $E_e\gtrsim 7$ MeV, our data analysis technique is not sensitive in sampling $M1$ strengths at higher energies where these transitions dominate.

The result of $\approx 19\mu_N^2$ for ^{239}Pu is compatible with those obtained for several odd actinides and a theoretical estimate for ^{239}U (Table I). However, the $M1+E2$ strength is insuf-

ficient to explain the cross section difference between 11 and 12 MeV, even when a *maximum* $E2$ strength is assumed (dash-dotted curve in Fig. 7). The maximum attainable $E2$ strength is obtained by assuming that $P_f^{E2}=1$. Although the $M1+E2$ (maximum) strength is substantially enhanced above 11 MeV, it still cannot match the experimental results. Moreover, the overall agreement below 11 MeV is worsened by such a procedure. Contributions to the electrofission process coming from higher order multipolar components (like $E3$), or from the onset of second-chance fission (threshold>12 MeV), are unlikely up to 12 MeV. It seems to us that $\Delta\sigma_{e,f}$ is overestimated between 11 and 12 MeV because our (γ,f) input [see Eq. (7)] is underestimated in this energy region. In fact, we note in Fig. 4 that the experimental photofission probability of ^{239}Pu is substantially lowered from $\approx$11 MeV till the $(\gamma,2n)$ threshold. On the other hand, by recalculating $\Delta\sigma_{e,f}$ between 11 and 12 MeV using a photofission cross section generated from the fitted $E1$ fission probability ($E1$ curve in Fig. 4), an agreement with the $M1+E2$ strength is dramatically achieved.

D. Calculation of the transition nucleus levels for ^{239}Pu

1. The semimicroscopic combined method

In order to calculate the transition levels for ^{239}Pu, we used the so-called semimicroscopic combined method [38,39]. This method uses the quantum statistical model proposed by Decowski *et al.* [40], which takes into account the shell and pairing effects calculated in the framework of the BCS model. However, this model does not give an adequate description of the level densities at low energies due to the discrete structure of the spectrum. Therefore, at low excitation energy, the level density calculation is carried out using a combinatorial method described in Ref. [38]. In both cases, realistic single particle spectra and phenomenological collective enhancement of the level densities in deformed nuclei are used. Since these calculations are carried out within the same model (BCS), and make use of the same single particle and pairing strengths parameters, a smooth joining of the discrete and continuous parts of the level densities is naturally achieved.

To check the applicability of the semimicroscopic combined method, the calculations were compared with experimental data for ^{239,240}Pu and ^{241,242}Am in the excitation energy range 0–10 MeV [39]. At the energy region corresponding to equilibrium deformation, the total level density of these nuclei was fully reproduced by these methods. At higher excitation energies (close to the neutron binding energy) the calculated level spacing is in good agreement with that from experiment [41], showing that this method can successfully be applied to describe level densities in a wide energy range. Moreover, the comparison of the experimental ^{239}Pu and ^{241}Am $\sigma(n,f)$ cross sections with the theoretical calculations showed that the combined method can describe also adequately the level density as a function of the nuclear deformation [39].

2. Calculation of the single particle spectra

The semimicroscopic combined method described above is very sensitive to the single particle spectrum; in particular, to the levels close to the Fermi energy. Therefore, an accurate calculation of the single particle states is necessary.

Due to difficulties in calculating the single particle spectrum for strongly deformed shapes, previous studies have generally taken methods appropriate to small deformations and applied them to larger deformations. Very recently, Garrote *et al.* [42] developed a more convenient approach to calculate the single particle states for strongly deformed nuclear shapes. According to this code (Cassini code), the deforming shape (up to and beyond its separation into two fragments) is described by the Cassinian ovals proposed by Pashkevich [43]. The Cassini code uses an axially deformed average Woods-Saxon potential which has been successfully applied to reproduce a number of single particle effects in strongly deformed nuclei (Ref. [44] and references therein).

In this work, the single particle spectra were obtained by means of the Cassini code using the Chepurnov parameters for the nuclear potential [45]. These parameters describe satisfactorily both neutron and proton single particle states.

Single particle spectra were calculated at the deformation region corresponding to the first saddle point of the fission barrier ($\epsilon=0.394$, $\alpha_4=-0.030$) as well as in the region of the second well ($\epsilon=0.505$, $\alpha_4=0.01$). The extreme points were calculated using the Struntinsky method [46] with Pashkevich parametrization of the nuclear shape [43]. Furthermore, the pairing strengths were taken to be $G_N=24.5A^{-1}$ MeV and $G_P=27.5A^{-1}$ MeV, respectively, for all the extreme points of the fission path.

3. Spectroscopy of the second well: A stringent test

The identification of single particle spectra in the second minimum is extremely important in order to test the single particle models at large deformations. Experimentally, the first results of spectroscopic investigations of fission isomers was reported in 1972 by Specht *et al.* [47], who identified a rotational band built on the 3.8 ns fission isomeric state in ^{240}Pu. Such rotational excitations have been latter identified (by conversion electron spectroscopy) for several other nuclei, including ^{239}Pu ([48] and references therein). Therefore, the reliability of our method at large deformations was checked by calculating single particle spectra at the deformation of the second well of the double-humped fission barrier and by comparing them with experimental results [49].

As we can see in Fig. 8, the agreement between the theoretical and experimental results is excellent, showing that the semimicroscopic combined method proposed in this work can be successfully used to calculate the single particle states at any deformation. In our calculations a rotational band with spin $5/2^+$ built on the 2.6 ns isomeric state in ^{239}Pu was obtained using the rotational constant $A=3.36$ keV given in Ref. [49]. As mentioned before, the deformation of the second well corresponds to $\epsilon=0.505$, $\alpha_4=0.01$.

More detailed results on the issue of spectroscopy of the second well for ^{239}Pu, as well as for some other odd actinides, will appear in a forthcoming publication [50].

4. Results and the issue of M1 strength in ^{239}Pu

From all calculated levels of the transition nucleus of ^{239}Pu, we show in Table II only those which could be ex-

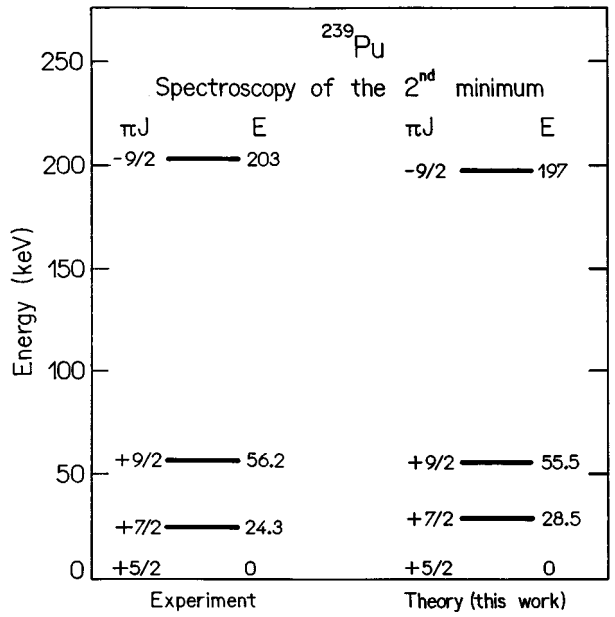

FIG. 8. Levels of the second minimum in the fission barrier of ^{239}Pu. Experimental results are from Ref. [49]. See text for the details of our theoretical calculations.

cited by $E1$, $M1$, and $E2$ transitions, and that are at the top of the higher inner barrier ($\epsilon=0.394$, $\alpha_4=-0.030$).

We assigned to the lowest level, $(J^\pi,K)=(\frac{3}{2}^-,\frac{3}{2})$, the photon excitation energy $\omega=5.35$ MeV, after a suggestion made by Vandenbosch and Huizenga [6] in their successful attempt to fit the experimental photofission angular distributions of ^{239}Pu. In fact, the best fit was achieved by assuming $(\frac{3}{2}^-,\frac{3}{2})$ as the lowest level at the first saddle, and as being excited by absorption of photons with $\omega=5.35$ MeV. Our results, plus the energy scaling mentioned above (at $\omega=5.35$ MeV), are qualitatively checked by means of a comparison with experimental angular distributions (next section).

Figure 9 presents the transition levels associated only with $E1$ and $M1$ transitions, for $\omega\leqslant 6.3$ MeV. The $E2$ strength is negligible below 7 MeV [see Fig. 3 (inset) and Fig. 6]. We observe a distinct bunch of three positive-parity levels at $5.5<\omega<5.9$ MeV (Fig. 8) which, as discussed above, could be associated only with $M1$ transitions. Our deduction of the $M1$ fission strength in ^{239}Pu (Sec. III C) indicates a concentration in the ω-interval of $(5.40\pm0.05)-(5.80\pm0.05)$ MeV, which is in good agreement with our theoretical findings. This agreement reinforces the fact that most of the strength responsible for $\Delta\sigma_{e,f}$ [Eq. (18), Fig. 3 (inset), and Fig. 7] is $M1$.

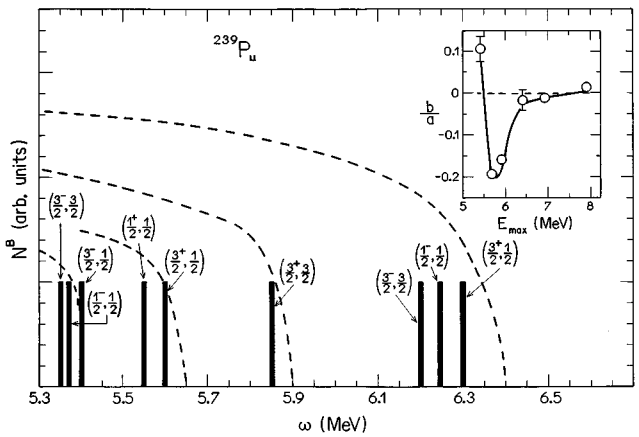

FIG. 9. Levels of the ^{239}Pu transition nucleus calculated in the present work. Only those levels associated with $E1$ and $M1$ transitions are presented. The dashed curves are pictorial representations of the Bremsstrahlung spectra, used in the experiment for the (γ,f) anisotropies of ^{239}Pu [17] shown in the inset ($E_{\max}$ is the energy of the Bremsstrahlung spectrum tip).

The levels of the second well (Fig. 8) are not included in our data analysis because of the extremely low isomeric fission cross section at energies above the fission barrier [5].

IV. (γ,f) ANGULAR DISTRIBUTIONS OF ^{239}Pu REVISITED

The photofission angular distributions of ^{239}Pu were measured with Bremsstrahlung at energies as low as 5.4 MeV [17,18]; these results are shown in Fig. 9.

The angular distribution functions $W^J_{M,K}(\theta)$ of odd-A nuclei for all the possible transition nucleus levels (J^π,K), and for all possible combinations of J, K, and M, can be put in the form [6]

$$W^J_K(\theta)=\sum_M W^J_{M,K}(\theta)=a+b\,\sin^2(\theta). \tag{21}$$

In the notation above, M is the projection of the angular momentum on the laboratory z axis, which coincides with the beam direction, and θ is the angle between the fission fragment trajectory and the beam direction.

Theoretical calculations for ^{239}Pu $(J^\pi_0=1/2^+)$ show that [6]

(a) $b<0$, for $(J,K)=(3/2,1/2)$,

(b) $b>0$, for $(J,K)=(3/2,3/2)$,

(c) $b=0$, for $(J,K)=(1/2,1/2)$.

The angular distributions do not differentiate positive- from negative-parity levels, since we are considering nonpolarized photon beams. However, the excitation of different K bands can be observed by the sign changes of the so-called ''anisotropy,'' b/a (a is always positive).

In this regard, we compare the results of our calculations for the transition levels (J^π,K) of ^{239}Pu with the experimental results for b/a [shown in Fig. 9 (inset)]. Since $E2$ excitations are hardly observed with real photons, we assume $E1$ and/or $M1$ excitations, only. In this case, ^{239}Pu decays by fission through the transition levels: $(1/2^+,1/2)$, $(3/2^+,1/2)$, $(3/2^+,3/2)$, and the same set of levels as before, but with negative parity. Thus the following conclusions can be drawn from Fig. 9: (1) A strong positive anisotropy $(b/a>0)$ at $E_{\max}=5.4$ MeV could be mostly attributed to the lowest $K=3/2$ transition level, excited by $E1$; it is important to note that the levels close to the tip ($E_{\max}$) of the Bremsstrahlung spectrum do not contribute appreciably to

TABLE II. Levels of the ^{239}Pu transition nucleus, as calculated in the present work.

E (MeV)	J^{π}	K	λL	ω (MeV)
$\gtrsim$ 0.01	$3/2^-$	3/2	E1	5.35
0.02	$1/2^-$	1/2	E1	
0.06	$3/2^-$	1/2	E1	5.40
0.21	$1/2^+$	1/2	M1/E2	
0.24	$5/2^+$	5/2	E2	
0.25	$5/2^+$	1/2	E2	
$\gtrsim$ 0.25	$3/2^+$	1/2	M1/E2	
0.54	$3/2^+$	3/2	M1/E2	5.85
$\gtrsim$ 0.58	$5/2^+$	3/2	E2	
$\gtrsim$ 0.86	$3/2^-$	3/2	E1	6.20
0.93	$1/2^-$	1/2	E1	
0.97	$5/2^+$	5/2	E2	
0.973	$5/2^+$	5/2	E2	
0.974	$5/2^+$	1/2	E2	
0.975	$3/2^+$	1/2	M1/E2	$\approx$ 6.30
0.978	$1/2^-$	1/2	E1	

M1-excitation*

*$E2$ strength$\approx$0, for $\omega<7$ MeV [see Fig. 3 (inset)].

the observed anisotropy; (2) For $E_{\max}=5.65$ MeV the anisotropy falls abruptly to a negative value, which could be explained by the two $K=1/2$ levels $(1/2^-,1/2)$ and $(3/2^-,1/2)$, near $\omega\approx5.4$ MeV and, to a lesser extent, to the levels $(1/2^+,1/2)$ and $(3/2^+,1/2)$ near the tip; (3) b/a increases only a little bit at $E_{\max}=5.9$ MeV, due to the presence of the level $(3/2^+,3/2)$ near the tip; (4) finally, towards $E_{\max}=6.4$ MeV, b/a approaches to zero quickly because, now, the levels with $K=3/2$, $(3/2^+,3/2)$, and $(3/2^-,3/2)$ are being intensively populated, plus the level $(1/2^-,1/2)$ which contributes to $b=0$. The level $(3/2^+,1/2)$ is too close to the tip.

For $E_{\max}>6.4$ MeV the number of levels with different K's are numerous enough to keep the anisotropy around zero.

Although qualitative, the comparison with the (γ,f) angular distributions shows that the transition levels we obtained theoretically are, quite probably, at the right energy positions, and that the corresponding J^{π} and K were properly assigned.

V. SUMMARY AND FINAL REMARKS

The results, data analysis and conclusions of this work are summarized as (1) the electrofission cross section of ^{239}Pu was measured in detail (steps of 0.25 MeV) in the interval 7–12 MeV; (2) kinematics considerations assured us that only the multipolar transitions $E1$, $E2$ $(T=0)$, and $M1$ are contributing to the (e,f) process; (3) from the well-known (γ,f) cross section of ^{239}Pu (taken from literature), the (e,f) $E1$ component was calculated and subtracted from the total (e,f) cross section (experimental data), generating thus the (e,f) cross section difference $\Delta\sigma_{e,f}$; (4) the cross section $\Delta\sigma_{e,f}$, corresponding to $E2$ $(T=0)$ and $M1$ transitions, was found to be $\sim$50% of the total (e,f) cross section for $E_e\lesssim8$ MeV. Such a substantial fraction of the total (e,f) process cannot be attributed to experimental and/or calculational uncertainties; (5) it was shown that the contribution of $E2$ $(T=0)$ to $\Delta\sigma_{e,f}$ is less than 10% for $E_e\lesssim8$ MeV, since only the low-energy tail of the GQR $(T=0)$ is present in this region; this fact greatly reduces most of the ambiguities generally associated with the analysis of inclusive data; (6) by considering that the $M1$ electrofission strength is $\approx0.9\Delta\sigma_{e,f}$, we deduced an $M1$ strength of $19\pm4\mu_N^2$ below 6 MeV; (7) the transition nucleus levels of ^{239}Pu were theoretically obtained; these results were favorably compared with photofission angular distributions from the literature; (8) also, these calculations showed a bunch of positive-parity levels in between $\approx$5.5–5.9 MeV, which certainly explains the concentration of $M1$ strength deduced in this work.

As final remarks, we note that the deduction of the $M1$ strength in ^{239}Pu was feasible due to some special conditions, particularly the concentration of the strength in the region corresponding to the low-energy tails of the GDR and the GQR $(T=0)$. Also, the fact that $N^{M1}\gg N^{E1}$ is responsible for a substantial (e,f) $M1$ strength below 7 MeV, like more than 40% of the total (e,f) cross section experimentally obtained. Finally, we stress that no attempt was made toward the decomposition of three multipoles. Actually, one of them was taken from the literature $(E1)$; another one, $E2$ $(T=0)$, was found to be small (below 8 MeV) affecting, thus, very little the data analysis; and only the remaining one, $M1$, was deduced.

All these special conditions of the experiment and data analysis ''attenuate,'' to a great extent, the most significant shortcoming of this work, namely, the $M1$ character is inferred only from the magnitude of the electrofission cross section, requiring thus a comparison with photofission data.

It is obvious that inclusive electrofission is not the best way to look for $M1$, since multipole assignment is not direct. However, there has been in the literature no news of an alternative effort toward the deduction of the $M1$ strength in the odd actinide mass region, where angular distributions are very difficult to measure.

ACKNOWLEDGMENTS

The authors thank the Brazilian agencies Conselho Nacional de Desenvolvimento Científico e Tecnológico (CNPq), Fundação de Amparo à Pesquisa do Estado de São Paulo (FAPESP), Financiadora de Projetos (FINEP), and Centro Latinoamericano de Física (CLAF-Brazil) for the partial financial support of this work (J.D.T.A.-N. was partially supported by FAPESP, São Paulo, Brazil, M.-L.Y. was supported by CNPq under Grant No. 301155/94-1, J.F.D. was supported by CNPq under Grant No. 301340/94-3, F.G. was supported by CNPq/CLAF under Grant No. 150052/96-0, and V.P.L. was supported by CNPq under Grant No. 300961/93-6). Moreover, we acknowledge the assistance of the students M. V. Tavares, V. S. Araújo, and W. S. Nishimoto in the early stages of this work.

[1] U. Kneissl, G. Kuhl, and A. Weller, Phys. Lett. **49B**, 440 (1974).
[2] U. Kneissl, G. Kuhl, K. H. Leister, and A. Weller, Nucl. Phys. **A256**, 11 (1976).
[3] A. C. Shotter, D. Branford, J. C. McGeorge, and J. M. Reid, Nucl. Phys. **A290**, 55 (1977).
[4] Th. Weber *et al.*, Nucl. Phys. **A150**, 1 (1990).
[5] M. L. Yoneama *et al.*, Nucl. Phys. **A604**, 263 (1996).
[6] R. Vandenbosch and J. R. Huizenga, *Nuclear Fission* (Academic, New York, 1973).
[7] J. D. T. Arruda-Neto, J. Phys. G **10**, 101 (1984).
[8] Th. Weber *et al.*, Phys. Lett. B **215**, 469 (1988).
[9] J. D. T. Arruda-Neto *et al.*, Nucl. Phys. **A389**, 378 (1982).
[10] C. Wagemans, *The Nuclear Fission Process* (CRC Press, Boca Raton, 1991).
[11] J. D. T. Arruda-Neto, A. Deppman, N. Bianchi, and E. De Sanctis, Phys. Rev. C **51**, 751 (1995).
[12] B. L. Berman *et al.*, Phys. Rev. C **34**, 2201 (1986).
[13] H. Dias, J. D. T. Arruda-Neto, B. V. Carlson, and M. S. Hussein, Phys. Rev. C **39**, 564 (1989).
[14] A. S. Iljinov, E. A. Cherepanov, and S. E. Chigrinov, Sov. J. Nucl. Phys. **32**, 166 (1980).
[15] C. M. Lederer and V. S. Shirley, *Table of Isotopes*, 7th ed. (Wiley, New York, 1978).
[16] J. D. T. Arruda-Neto, Phys. Rev. C **29**, 1905 (1984).
[17] N. S. Rabotnov *et al.*, Nucl. Phys. **77**, 92 (1966).
[18] A. S. Soldatov, Yu. M. Tsipenyuk, and G. N. Smirenkin, Sov. J. Nucl. Phys. **11**, 552 (1970).
[19] J. D. T. Arruda-Neto *et al.*, Phys. Scr. **40**, 735 (1989).
[20] J. D. T. Arruda-Neto *et al.*, J. Phys. G **11**, 649 (1985).
[21] J. D. T. Arruda-Neto, S. L. Paschoal, and S. B. Herdade, J. Phys. G **14**, 373 (1988).
[22] D. Bohle *et al.*, Phys. Lett. **137B**, 27 (1984).
[23] A. Richter, Nucl. Phys. **A522**, 139 (1991).
[24] A. Richter, Prog. Part. Nucl. Phys. **34**, 261 (1995).
[25] S. Raman, L. W. Fagg, and R. S. Hicks, Int. Rev. Nucl. Phys. **7**, 355 (1991).
[26] R. Köhler *et al.*, Phys. Rev. C **35**, 1646 (1987).
[27] R. M. Laszewski, R. Alarcon, D. S. Dale, and S. D. Hoblit, Phys. Rev. Lett. **61**, 1710 (1988).
[28] R. S. Hicks *et al.*, Phys. Rev. C **26**, 920 (1982).
[29] A. van der Woude, Prog. Part. Nucl. Phys. **18**, 217 (1987).
[30] J. D. T. Arruda-Neto, S. B. Herdade, and I. C. Nascimento, Nucl. Phys. **A334**, 297 (1980).
[31] F. Zamani-Noor and D. S. Onley, Phys. Rev. C **33**, 1354 (1986).
[32] J. D. T. Arruda-Neto *et al.*, Phys. Rev. C **29**, 2399 (1984).
[33] J. D. T. Arruda-Neto, W. Rigolon, and S. B. Herdade, Phys. Scr. **35**, 427 (1987).
[34] A. S. Iljinov *et al.*, Nucl. Phys. **A543**, 517 (1992).
[35] E. F. Gordon and R. Pitthan, Nucl. Instrum. Methods **145**, 569 (1977).
[36] J. D. T. Arruda-Neto and B. L. Berman, Nucl. Phys. **A349**, 483 (1980).
[37] G. A. Bartholomew *et al.*, Adv. Nucl. Phys. **7**, 229 (1973).
[38] F. Garcia, O. Rodriguez, E. Garrote, and E. Lopez, J. Phys. G **19**, 2157 (1993).
[39] F. Garcia, O. Rodriguez, V. A. Rubchenya, and E. Garrote, Comput. Phys. Commun. **86**, 129 (1995).
[40] P. Decowski *et al.*, Nucl. Phys. **A110**, 129 (1968).
[41] S. F. Mughabghab and D. I. Garbu, Report No. BNL-NCS-325, 1973.
[42] E. Garrote, R. Capote, and R. Pedrosa, Comput. Phys. Commun. **92**, 267 (1995).
[43] V. V. Pashkevich, Nucl. Phys. **A169**, 275 (1971).
[44] S. Cwiok *et al.*, Comput. Phys. Commun. **46**, 379 (1987).
[45] V. A. Chepurnov, Sov. J. Nucl. Phys. **6**, 696 (1968).
[46] V. M. Strutinsky, Nucl. Phys. **A95**, 240 (1967).
[47] H. J. Specht, J. Weber, E. Konecny, and D. Heunemann, Phys. Lett. **41B**, 43 (1972).
[48] D. Habs, Nucl. Phys. **A502**, 105c (1989).
[49] H. Backe and L. Richter, Phys. Rev. Lett. **42**, 490 (1979).
[50] J. D. T. Arruda-Neto *et al.*, in preparation.
[51] J. D. T. Arruda-Neto, S. B. Herdade, and B. L. Berman, J. Phys. G **12**, 105 (1986).
[52] C. S. Shapiro and G. T. Emery, Phys. Rev. Lett. **23**, 244 (1969).
[53] M. A. P. V. de Moraes and M. F. Cesar, Nucl. Instrum. Methods Phys. Res. A **277**, 467 (1989).
[54] D. Zawischa and J. Speth, in *Proceedings of the International Symposium on ''Nuclear Fission and Related Collective Phenomena and Properties of Heavy Nuclei''*, Bad Honnef, Germany, 1981, edited by P. David, T. Mayer-Kuckuk, and A. van der Woude, Lecture Notes in Physics Vol. 158 (Springer-Verlag, Berlin, 1982), p. 231.